Impact of hydraulic sorting and weathering on mica provenance studies: An example from the Yangtze River

Impact of hydraulic sorting and weathering on mica provenance studies: An example from the Yangtze River

Xilin Sun[a,b,c,*], K.F. Kuiper[c,**], Yuntao Tian[a,b,*], Chang'an Li[d], L. Gemignani[c,e], Zengjie Zhang[a,f], J.R. Wijbrans[c]

[a] Guangdong Provincial Key Laboratory of Geodynamics and Geohazards, School of Earth Sciences and Engineering, Sun Yat-Sen University, Guangzhou 510275, China
[b] Southern Marine Science and Engineering Guangdong Laboratory (Zhuhai), Zhuhai 519082, China
[c] Cluster Geology and Geochemistry, Vrije Universiteit Amsterdam, De Boelelaan 1085, 1081 HV Amsterdam, the Netherlands
[d] School of Earth Sciences, China University of Geosciences, Wuhan 430074, China
[e] Department of Earth Science, Freie Universität Berlin, Berlin, Germany
[f] CAS Key Laboratory of Ocean and Marginal Sea Geology, Guangzhou Institute of Geochemistry, Chinese Academy of Sciences, Guangzhou, China

ARTICLE INFO

Editor: Jérôme Gaillardet

Keywords:
Muscovite
Biotite
Provenance
Grainsize
Age population
Yangtze River

ABSTRACT

Detrital muscovite and biotite $^{40}Ar/^{39}Ar$ analyses are useful tools for studying regional tectonic histories, sediment provenances and paleo-drainage reconstructions. During transport and recycling of detrital micas physical and chemical weathering occurs. This process effects the grain size and age populations ultimately found in river sediments, but is often ignored in provenance studies. Here, we present detrital muscovite and biotite $^{40}Ar/^{39}Ar$ results of 15 modern sediments from the Yangtze River to address the impact of grainsize on provenance age populations. The beam intensities of ^{39}Ar, formed from ^{39}K by neutron capture reaction during sample irradiation, have been used as an index for grain size. We found that relatively older detrital mica ages of the Yangtze River are often characterized by small ^{39}Ar signals (i.e., grain sizes), and large grain sizes correspond to younger grains. This observation is also revealed by reanalysis of previously reported detrital mica studies in other major river systems (Red and Brahmaputra rivers) and sediments (Scotian Basin, Canada and Antarctic) and probably results from physical and chemical weathering during transport and recycling. Our Yangtze results indicate that detrital muscovite and biotite ages of grainsize ranging from 100 to 1000 μm cover all age components as identified in all dated grains (with a size of > 100 μm), and thus indicate that detrital mica $^{40}Ar/^{39}Ar$ analyses should include also small grains from > 100 μm to reduce the effects of hydraulic sorting and weathering. Grainsizes smaller than 100 μm have not been tested in this study, but will be more difficult to date due to both smaller beam intensities and possible recoil effects.

1. Introduction

With the development of laser microanalysis and high sensitivity multi-collector noble gas mass spectrometers, $^{40}Ar/^{39}Ar$ ages of detrital minerals (muscovite, biotite, amphibole, K-feldspar and hornblende) become a popular provenance tool for constraining sediment provenance and bedrock erosion, depositional age and paleo-drainage reconstruction (Chetel et al., 2005; Clift et al., 2006; Gemignani et al., 2018; Gwiazda et al., 1996; Haines et al., 2004; Hodges et al., 2005; McDougall and Harrison, 1999; Pierce et al., 2014; Reynolds et al., 2009; Uddin et al., 2010). Detrital muscovite and biotite, commonly used for $^{40}Ar/^{39}Ar$ analyses, are less resistant to physical abrasion and chemical dissolution than rutile, monazite and zircons, other widely used minerals for detrital U—Pb analyses (Haines et al., 2004; Parrish, 1990; Újvári et al., 2013). Provenance studies of detrital zircons reveal a notion that younger zircons have coarser and more variable sizes than the older zircons (Lawrence et al., 2011; Malusà et al., 2013; Malusà et al., 2016; Sircombe et al., 2001; Yang et al., 2009). Such an effect probably also exists in detrital micas, but has not been well explored by detailed studies.

Detrital grains are effectively sorted by their shape, density and size (Garzanti et al., 2008, 2009). As to micas, on one hand, shape of mica (platy mineral) plays a fundamental role in hydrodynamic sorting, which concentrates micas in coarser fraction (Garzanti et al., 2009). On

* Corresponding authors at: Guangdong Provincial Key Laboratory of Geodynamics and Geohazards, School of Earth Sciences and Engineering, Sun Yat-Sen University, Guangzhou 510275, China.
** Corresponding author.
E-mail addresses: sunxlin3@mail.sysu.edu.cn (X. Sun), k.f.kuiper@vu.nl (K.F. Kuiper), tianyuntao@mail.sysu.edu.cn (Y. Tian).

https://doi.org/10.1016/j.chemgeo.2019.119359
Received 16 April 2019; Received in revised form 27 October 2019; Accepted 2 November 2019
Available online 06 November 2019

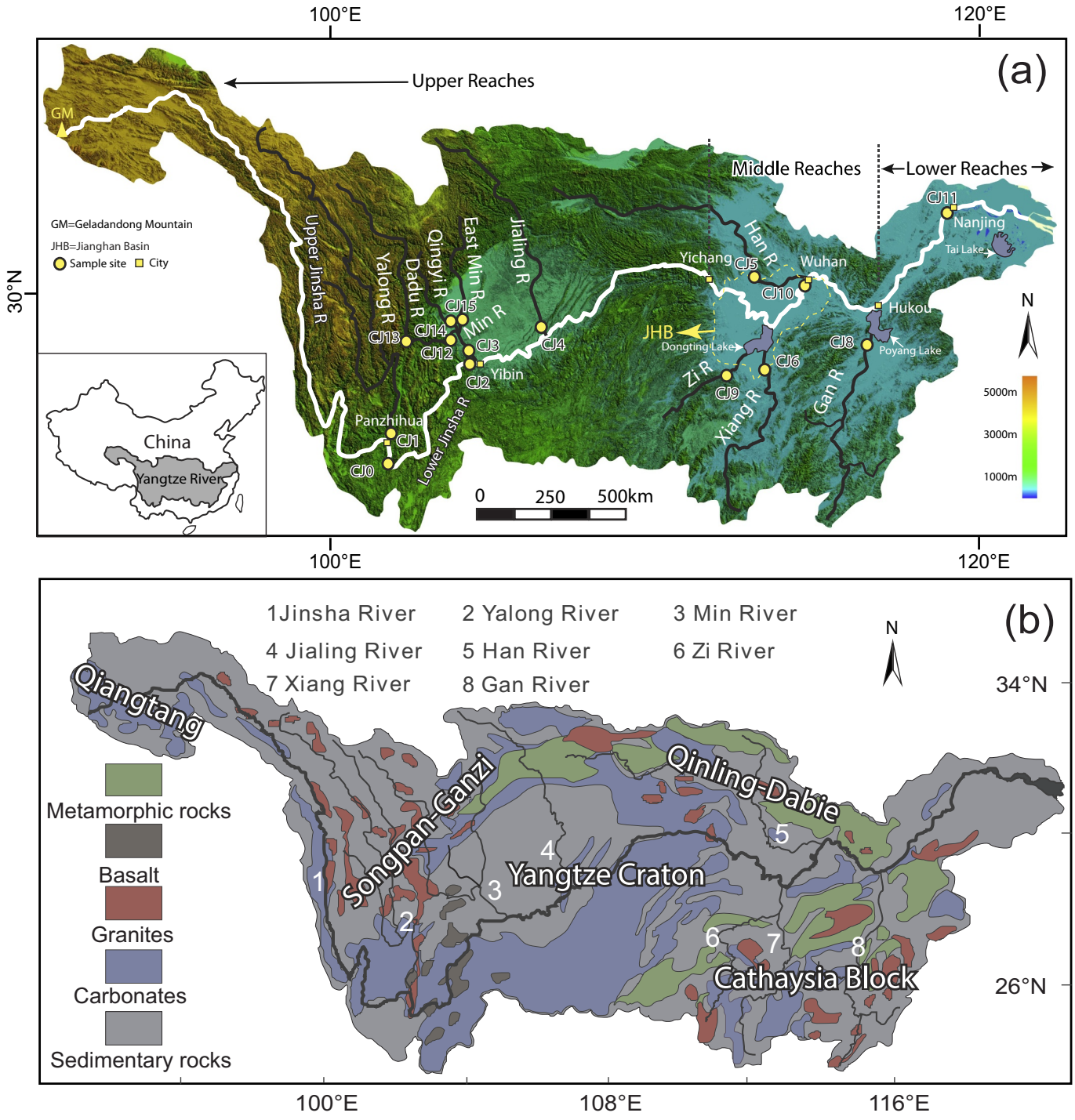

Fig. 1. a) Schematic map showing the drainage and sampling locations; b) generalized geological map of the Yangtze River. JHB: Jianghan Basin. The Dadu, Qingyi and East Min rivers are three tributaries of the Min River.

the other hand, due to physical and chemical weathering, mica grain size decreases with increasing of transport distance and sediment reworking cycles. Thus, smaller micas are expected to source from distant and/or older areas, and large grains originate from nearby and/or younger areas. When dating micas from a certain grain size range, some age populations might be underestimated or even missed. Such a potential bias has been shown to exist for detrital zircon U−Pb analyses (Lawrence et al., 2011; Sircombe et al., 2001; Yang et al., 2009). Previous studies used different mica size ranges for provenance study, for example 250-500 μm (Carrapa et al., 2004; Hoang et al., 2010), 300–1000 μm (Reynolds et al., 2009), 125-1000 μm (Gemignani et al., 2019) or > 1000 μm (Stuart et al., 2001; Uddin et al., 2010). If the mica age populations are indeed dependent upon grain size, age results using incomplete size ranges will be compromised and require more information on the effects of hydraulic sorting on detrital mica age distribution. Here, we are in particular interested if the 100–250 /300 μm size fraction holds information that might be missed if only focusing on the larger grainsize fractions.

The Yangtze River (Fig. 1), as the largest river in Asia, is a suitable candidate for assessing hydraulic sorting on detrital mica age distribution. Its sediment provenances have been intensively studied by numerous methods, including zircon U−Pb, Pb isotopes of K-feldspar,

monazite U-Th-Pb, clay mineral composition, Nd isotopes and heavy minerals composition (Fan et al., 2005; He et al., 2013a; He et al., 2013b; Jia et al., 2010; Shao et al., 2012; Sun et al., 2016; Wang et al., 2010; Yang et al., 2009; Zhang et al., 2016). Further, previous studies have also reported a large amount of detrital muscovite $^{40}Ar/^{39}Ar$ ages (Hoang et al., 2010; Sun et al., 2016) from its trunk and major tributaries.

In this study, we report new biotite $^{40}Ar/^{39}Ar$ ages ($n = 470$) and compiled our previously reported muscovite data ($n = 687$, Sun et al., 2016) from the Yangtze R iver. Mica size measurements have been performed using microscopy for 111 grains to calibrate the relationship between grain size and $^{39}Ar_K$ beam intensities that is produced from ^{39}K by neutron capture reaction during sample irradiation. This time-saving way is utilized to test the hydraulic sorting effect on micas. We also aim to determine the most representative grain size window for mica $^{40}Ar/^{39}Ar$ ages for the Yangtze River system.

2. Geological setting and sampling

The Yangtze River is primarily situated in the Yangtze Craton, surrounded by the Qiangtang Block to the southwest, the Songpan-Ganzi Block to the west, the Qinling-Dabie orogen to the northwest and north and the Cathaysia Block to the east (Fig. 1b). The catchment drains a variety of rocks, including Archean and Proterozoic metamorphic and igneous rocks, Paleozoic carbonate, Mesozoic-Cenozoic igneous and siliciclastic rocks and Quaternary sediments (China Geological Survey, 2004).

The major tributaries of the Yangtze River are characterized by different tectonic settings and bedrocks. These are, from upstream to downstream (Fig. 1b), (1) the Jinsha River basin, comprising Triassic low-grade metamorphic rocks, Paleozoic carbonate, clastic and volcanic rocks (Reid et al., 2005; Wu et al., 2009). Sample CJ0 were collected from the downstream of the Yalong-Jinsha confluence and sample CJ2 are from the upstream of the Min-Jinsha confluence (Fig. 1a). (2) The Yalong (sample CJ1) and Min (sample CJ3) rivers draining the Songpan-Garze Block consisting of deformed and locally metamorphosed Middle to Late Triassic turbidites and numerous Triassic and Cenozoic intrusions (Roger et al., 2010; Xu et al., 1992). Samples CJ12 - CJ15 are sampled from three major tributaries of the Min River. (3) The Jialing River (sample CJ4) drainage area comprises Jurassic red beds and Quaternary loess deposits. (4) The Han River basin (sample CJ5) is characterized by metamorphic rocks, carbonate, the Mesozoic intrusions and clastics (Dong et al., 2011). (5) The Xiang (sample CJ6) and Zi rivers (sample CJ9) contain mostly Proterozoic medium-low grade metamorpic and carbonate rocks, and Jurassic - Quaternary terrestrial sediment (Shu et al., 2011). (6) The Gan River (sample CJ8) is located in the Cathayia block, which contains outcrops of old medium-low grade metamorphic rocks, carbonate rocks, and Quaternary clastic sediment. Detailed geological information on the Yangtze bedrocks can be found in He et al. (2013a) and Vezzoli et al. (2016). Two samples (CJ10 and CJ11) were collected from the main stream of the Yangtze near Wuhan and Nanjing cities for sampling signals of the entire Yangtze (Fig. 1).

A total of 15 samples cover most major tributaries. Sites where landslide features can be identified or reported are avoided. Our sampling sites are also selected to be at least 2 km away from small tributaries to avoid local bias towards a particular source. All samples (~2–4 kg each) were collected from the top 10 cm of newly-deposited sediments from river sand bars. Our samples include different hydrodynamic environments of each sand bar by randomly selecting 2–4 sampling sites on the targeted bar to avoid hydrodynamic fractionation of minerals as found by Lawrence et al. (2011). Details of all samples are given in Table 1.

Table 1
Summary of sample information.

Type	Number	Rivers	Longitude	Latitude	Locations
Tributary	CJ1	Yalong River	101°48′01″	26°36′29″	Panzhihua
	CJ3	Min River	104°33′46″	28°48′26″	Yibin
	CJ4	Jialing River	106°23′49″	29°53′13″	Beibei
	CJ5	Han River	112°33′30″	31°11′09″	Zhongxiang
	CJ6	Xiang River	112°55′19″	28°03′10″	Changsha
	CJ8	Gan River	115°51′21″	28°40′50″	Nanchang
	CJ9	Zi River	112°18′13″	28°36′54″	Yiyang
	CJ12	Dadu	103°33′11″	29°24′58″	Leshan
	CJ13	Dadu	101°20′55″	29°13′38″	Shimian
	CJ14	Qingyi	103°41′17″	29°35′30″	Leshan
	CJ15	East Min	103°24′58″	29°37′17″	Leshan
Mainstream	CJ0	Jinsha River	101°53′01″	25°57′45″	Yuanmou
	CJ2	Jinsha River	104°36′13″	28°45′04″	Yibin
	CJ10	Yangtze River	30°39′41″	114°23′24″	Wuhan
	CJ11	Yangtze River	32°10′02″	118°50′05″	Nanjing

3. Analytical methods

3.1. Electron microprobe analysis

Muscovite and biotite (> 100 μm) were separated from the 15 samples using conventional heavy liquid and magnetic separation techniques. Samples were handpicked under a binocular microscope to remove grains with signs of visible weathering or inclusions. The muscovite and biotite fractions were randomly split into two aliquots for chemical analysis and age determinations. The muscovite and biotite grains from the first aliquot were embedded in epoxy resin, polished to expose an internal surface and carbon coated for electron microprobe analysis. The major element geochemistry of muscovite and biotite grains was determined by JEOL JX-A8800M electron microprobe at Vrije Universiteit Amsterdam (Fig. 2a-d). Wavelength dispersive spectrometers were used with 20 nA beam current and 15 kV accelerating voltage.

3.2. Volume of single muscovite and biotite grain

In this study, we use $^{39}Ar_K$ beam intensities as a proxy for muscovite or biotite grain size. For this purpose, it is necessary to establish a correlation between grain volume and ^{39}Ar signal. Weighting the single mica grains proved to be difficult due to the small grain size and the static nature of the micas. In order to measure grain volume, we use a microscope and micrometer scale (precision = ~1 μm) to determine area and thickness of a series of grains (Appendix A). The grain volume of a single platy muscovite or biotite grain is determined as the product of plate area and thickness. We randomly choose muscovite and biotite grains for volume measurements from each of six samples from different portions of the Yangtze River, including sample CJ11 from the lower reaches near Nanjing, CJ10 from the middle reaches near Wuhan, and CJ2, CJ3, CJ12 and CJ13 from its upper tributaries.

To facilitate grain thickness measurements, we first placed a randomly picked single grain between a glass slide and a coverslip to measure the total thickness using the micrometer. Then, by subtracting the slide and coverslip thickness, the grain thickness is determined. Based on image taken by microscope (Nikon Eclipse 50i POL), the area of each grain was calculated using imaging software NIS-Elements D.

3.3. Muscovite and biotite $^{40}Ar/^{39}Ar$ dating

The $^{40}Ar/^{39}Ar$ dating is a variant of the $^{40}K/^{40}Ar$ method, based on the decay of radioactive ^{40}K into ^{40}Ar. $^{40}Ar/^{39}Ar$ dating relies on neutron irradiation in a nuclear reactor to transform a stable form of potassium (^{39}K) into the ^{39}Ar to be analyzed in a mass spectrometer together with ^{40}Ar. A standard of known age is irradiated with sample to

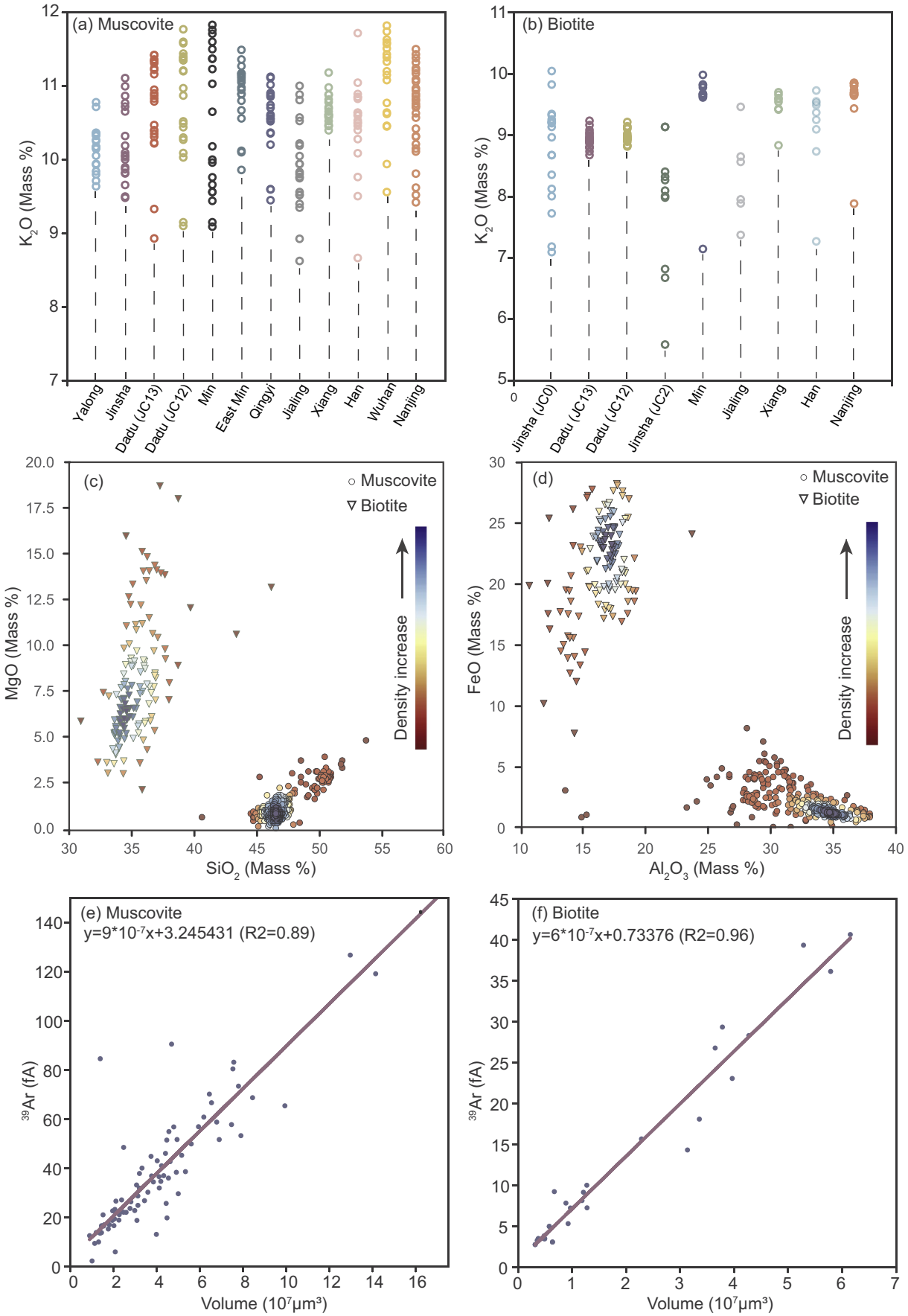

Fig. 2. The variation in K_2O content of detrital muscovite (a) and biotite (b) grains in the Yangtze River. Muscovite and biotite compositions: MgO against SiO_2 (c) and FeO against Al_2O_3 (d). Linear correlation between ^{39}Ar and grain volume of detrital muscovite and biotite grains (e and f). Note: two regression lines do not go through the origin because overestimation of each grain volume due to non-ideally flat surface.

Table 2
Argon sensitivity of AGES and Helix Mc based on international standard HD-B1 biotite.

Facility	Number	HD-B1 (mg)	Mol of ^{40}Ar	$^{40}Ar^*$ (cps)	Mol/cps
AGES	HD-B1_B3	1.01	3.434×10^{-13}	529,760	6.482×10^{-19}
	HD-B1_C3	2.00	6.8×10^{-13}	932,985	7.288×10^{-19}
	HD-B1_D3	3.13	1.0642×10^{-12}	1,684,985	6.316×10^{-19}
	HD-B1_E3	4.15	1.411×10^{-12}	2,119,826	6.565×10^{-19}
	HD-B1_A4	4.96	1.6864×10^{-12}	2,206,668	7.642×10^{-19}
	HD-B1_B4	6.66	2.2644×10^{-12}	2,792,153	8.109×10^{-19}
Average					$(7.08 \pm 0.29) \times 10^{-19}$

Facility	Number	HD-B1 (mg)	Mol of ^{40}Ar	^{40}Ar *(fA)	mol/fA
Helix-MC	HD-B1-E7_3	0.082	2.788×10^{-14}	77.970	3.575×10^{-16}
	HD-B1-F7_5	0.119	4.046×10^{-14}	112.106	3.609×10^{-16}
	HD-B1-G7_6	0.078	2.652×10^{-14}	80.395	3.298×10^{-16}
	HD-B1-H7_3	0.126	4.284×10^{-14}	124.561	3.439×10^{-16}
	HD-B1-I7_4	0.210	7.14×10^{-14}	183.771	3.855×10^{-16}
	HD-B1-J7_5	0.267	9.078×10^{-14}	279.497	3.248×10^{-16}
	HD-B1-K7_7	0.309	1.0506×10^{-13}	307.872	3.141×10^{-16}
	HD-B1-L7_8	0.630	2.142×10^{-13}	640.822	3.423×10^{-16}
Average					$(3.48 \pm 0.07) \times 10^{-16}$

Note: the ^{40}Ar of Helix is measured on the H2 Faraday cup equipped an $10^{12}\Omega$ amplifier. The radiogenic $^{40}Ar^*$ of HD-B1 is $3.444 \pm 0.033 \times 10^{-10}$ mol/g.

identify the integrated neutron flux that the sample has received (neutron flux variation: J).

For irradiation, each grain whose dimensions were determined was individually wrapped in a numbered ~2 mm Al-foil package. All these small packages from one sample were sealed in 6 mm diameter Al-foil package for irradiation. For each sample, additional grains (without volume measurements) were sealed into a 6 mm diameter Al-foil package for irradiation. Samples were irradiated for 18 h in CLICIT Facility in Oregon State University Radiation Center with an in-house standard, Drachenfels sanidine (DRA; 25.52 ± 0.08 Ma) (Wijbrans et al., 1995, calibrated to Kuiper et al., 2008), to measure the neutron flux variation (J).

Total fusion $^{40}Ar/^{39}Ar$ ages of detrital muscovite and biotite grains were dated at argon geochronology laboratory of the Vrije Universiteit Amsterdam (Appendix B). Details of muscovite and biotite $^{40}Ar/^{39}Ar$ age determinations are given in Sun et al. (2018). Muscovite and biotite grains were analyzed using either a ThermoFisher Helix MC multi-collector (Helix MC) noble gas mass spectrometer or a Hiden HAL 3F Series 1000 Pulse Ion Counting Triple Filter quadrupole mass spectrometer (AGES). The units of output data from the two mass spectrometers are different (Helix MC: femtoampere and AGES: count per second). To facilitate the comparison, we convert the ^{39}Ar signal of detrital mica grains from the AGES to a femtoampere (fA) unit. To do so, it is required to determine the sensitivities of the two kinds of mass spectrometers, which was calibrated using the HD-B1 biotite, an international standard with an age of 24.7 ± 0.3 Ma, a K content of 7.985 ± 0.023 (wt%) and a radiogenic ^{40}Ar content of $3.444 \pm 0.033 \times 10^{-10}$ mol/g (Fuhrmann et al., 1987; McDougall and Harrison, 1999). Analytic results of multiple fusion experiment of HD-B1 on both our Helix MC and quadrupole system (AGES) are given in Table 2. Average sensitivities of Helix MC and AGES are respectively $\alpha_{(Helix)} = (3.48 \pm 0.07) \times 10^{-16}$ mol/fA and $\alpha_{(AGES)} = (7.08 \pm 0.29) \times 10^{-19}$ mol/cps, respectively. Since most of our measurements were performed on our Helix, we report our data in fA, using a conversion factor of 2.034×10^{-3} fA/cps ($\alpha_{Helix}/\alpha_{AGES}$) for the AGES data. J values of bracketing standards (DRA) were used to normalize the $^{39}Ar_K$ values of grains from different samples to an integrated neutron flux.

4. Results

The Potassium contents of muscovite and biotite grains were determined by JEOL JX-A8800M electron microprobe. Potassium contents of muscovite and biotite grains from our samples fall in a rather narrow range (Ms: 9.0 ± 0.45–12.0 ± 0.6% and Bt: 6.0 ± 0.3–10.5 ± 0.52%) (Fig. 2a and b), suggesting that K contents are consistent among our samples. During irradiation ^{39}K in a sample is converted to $^{39}Ar_K$. Variations in measured $^{39}Ar_K$ is therefore mainly a result of different K compositions of individual grains, grain size and duration of irradiation as calculated with the following equation (see Table 3).

$$^{39}Ar_K = \frac{J \times \frac{\lambda_\varepsilon}{\lambda} \times x \times y \times z \times \rho \times \frac{K_2O \times 2}{\text{atomic mass } K_2O} \times \frac{^{40}K}{K}/100}{\text{Sensitivity}}$$

With J is 0.0045, λ_e/λ is the branching ratio of the decay constants, x, y and z defines thickness of the mineral, K_2O in wt%, $^{40}K/K$ is atomic abundance of 0.0001167 and the sensitivity is $3.48*10^{-16}$ mol/fA. From Fig. 3a and Table 3 it is easily seen that the effect of grain size has a much larger impact on ^{39}Ar variations than the range in K_2O composition. We therefore argue that ^{39}Ar is a valid proxy for grain size. This is confirmed by our data in Fig. 2e and f that shows a linear correlation (Ms: $R^2 = 0.89$ and Bt: $R^2 = 0.96$) between calibrated ^{39}Ar signals against grain volumes of muscovite or biotite grains, as is expected from our theoretical calculations. This justifies our approach to use $^{39}Ar_K$ beam intensities as a proxy for grain volume.

Our new single grain biotite $^{40}Ar/^{39}Ar$ ages are all younger than 900 Ma clustering at three age peaks around 600–900 Ma, 160–250 Ma and 0–60 Ma (Fig. 4a and c), similar to our previously reported muscovite results (Sun et al., 2016). Plotting of our previously reported muscovite (Sun et al., 2016) and newly acquired biotite ages against ^{39}Ar signals (or grain size) shows that > 99% data points fall within the lower left part of the figure (Fig. 4b and d). The ^{39}Ar signals of the oldest muscovite age population (700–1750 Ma) are consistently small (< 20 fA). In addition, mica grains of the young age components (< 250 Ma) have a wide range of ^{39}Ar signals (0–120 fA) and volumes.

Table 3
Estimated $^{39}Ar_K$ (in fA) for different K_2O contents and grain size assuming J is 0.0045 and sensitivity is $3.48*10^{-16}$ mol/fA (Fig. 3a).

Content of K	Grain size (μm) of 100 × 100 × 20	Grain size (μm) of 500 × 500 × 20	Grain size (μm) of 1000 × 1000 × 20
6.0 wt% K_2O	0.11	2.83	11.33
9.0 wt% K_2O	0.17	4.25	16.99
10.5 wt% K_2O	0.20	4.96	19.83
12.0 wt% K_2O	0.23	5.66	22.66

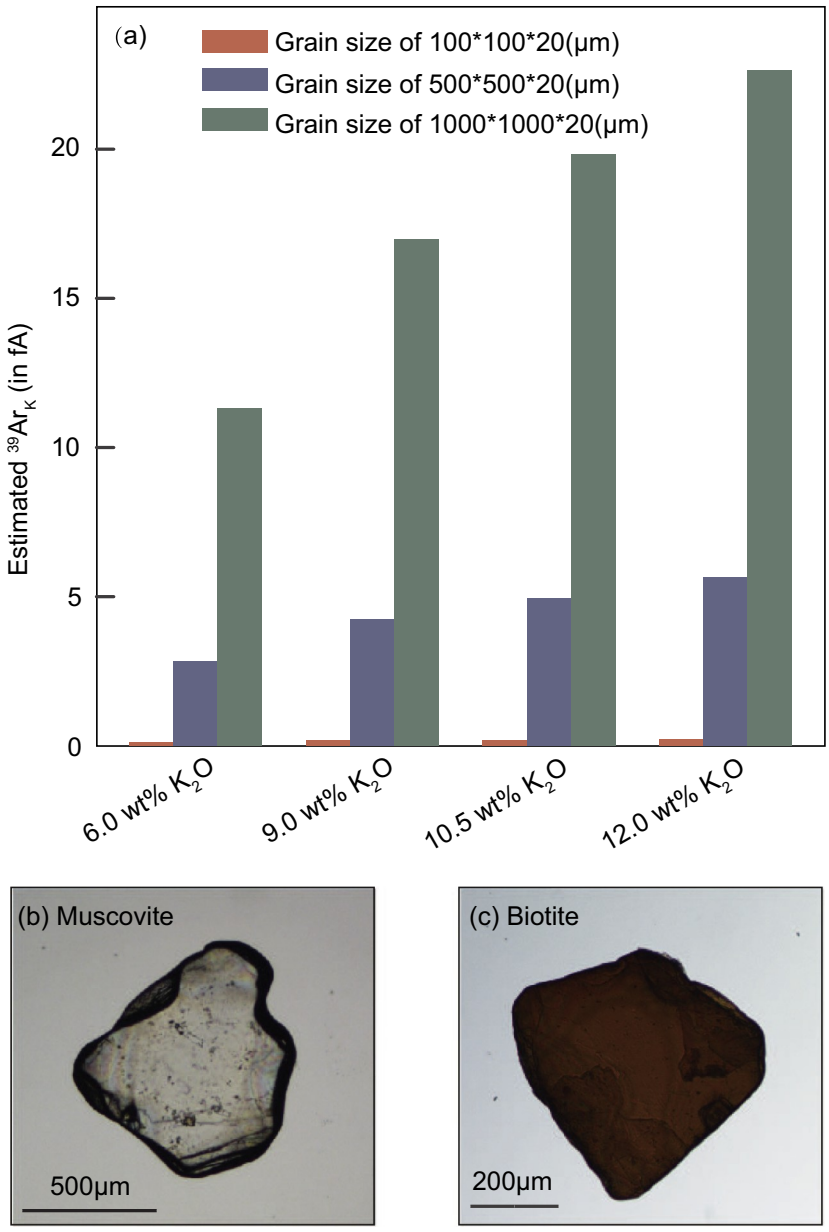

Fig. 3. a) Estimated $^{39}Ar_K$ for different K_2O contents and grain size, assuming J value is 0.0045 and sensitivity for mass spectrometer is $3.48*10^{-16}$ mol/fA. Data of this figure is presented in the Table 3. b) and c) Representative microscopic pictures of muscovite and biotite grains used for determining the relationship between grain volume and ^{39}Ar signal.

We also compared the age spectra and cumulative density functions for different grain sizes (Fig. 5). It is found that the age distribution strongly depends on the mica grain sizes. The age distributions of grains > 1000 μm is remarkably different from the distribution based on all dated grains (> 100 μm range) and slightly different from those of 500–1000 μm and 200–500 μm. These results have important implications for mica hydraulic sorting and its effect on detrital $^{40}Ar/^{39}Ar$ age analysis, which will be discussed below.

5. Discussion

5.1. Multiple recycling

The Yangtze River data set shows a trend that relatively older micas are generally smaller and larger micas are younger (Fig. 4b and d). This trend could be inherited from either host rocks or progressive abrasion during multiple recycling and transport. The relation between grain size and age in host rocks has been tested empirically in studies based on biotite and white mica grains from plutons (Alexandre, 2011) and metamorphic rocks (Markley et al., 2002; Uunk et al., 2018). A commonly observed trend of grain size - age relationships of mica grains in the host rocks is that total fusion ages increase with grain size due to diffusion of ^{40}Ar out of the mineral with smaller grains more severely affected by diffusion than larger grains. Such a relationship is different from our observed trend in detrital micas age versus grain size populations.

We suggest that the grain size - age trend results from sediment multiple recycling. Micas in the Yangtze River are mostly sourced from upstream areas (Hoang et al., 2010; Sun et al., 2016), that mainly consist of Triassic Songpan-Ganze flysch deposits (Fig. 1b). Many studies suggest that the detritus in these areas is derived from Paleozoic and pre-Cambrian crystalline and sedimentary rocks of the Qinling-Dabie orogen and South China block (Enkelmann et al., 2006; Weislogel et al., 2010; Weislogel et al., 2006; Yan et al., 2019). Therefore, current

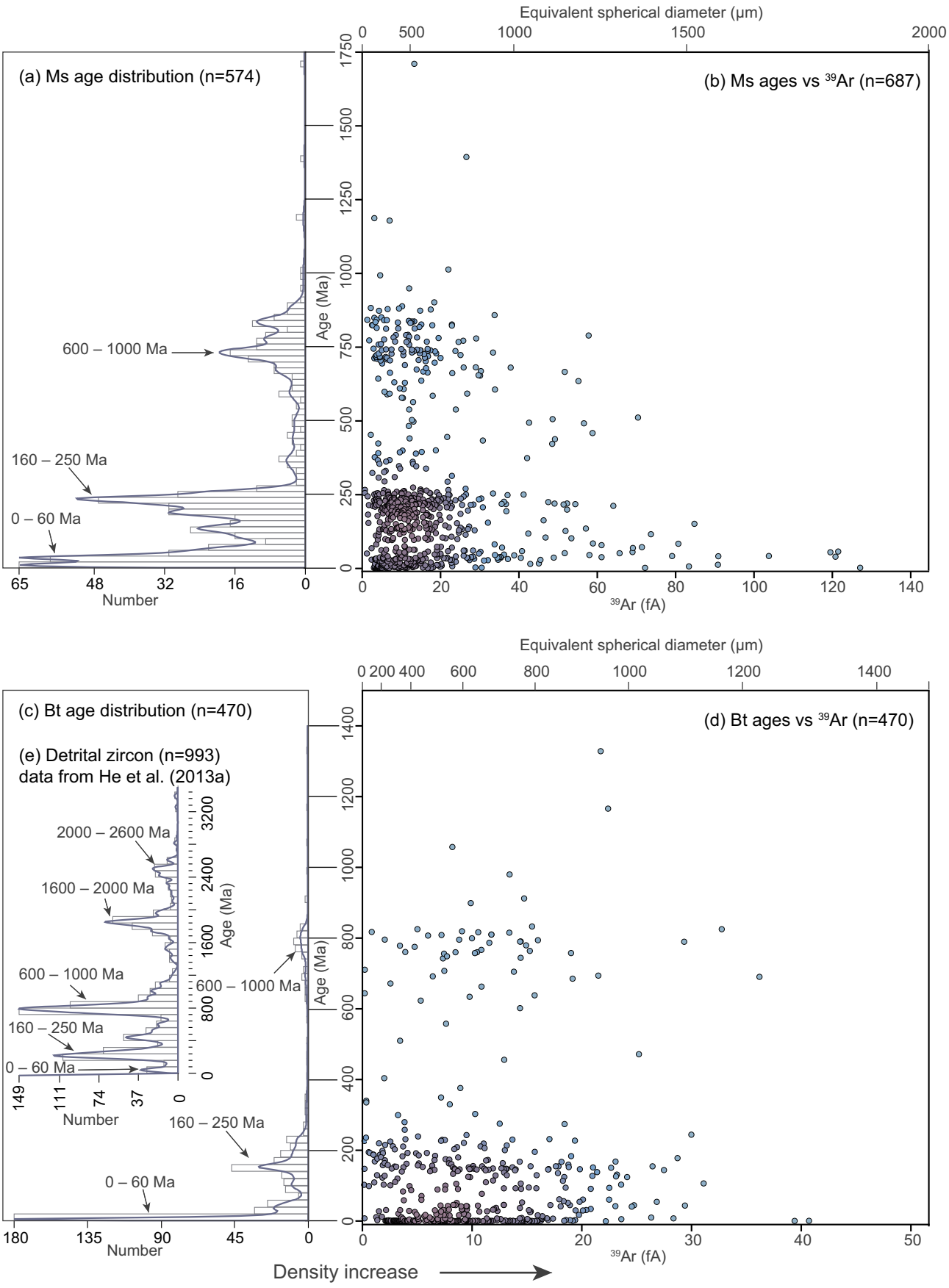

(caption on next page)

Fig. 4. Detrital muscovite, biotite and zircon age distributions (a, c and e). Detrital zircon data from He et al. (2013a). Age – grain size correlation of detrital muscovite (b) and biotite (d) grains from the Yangtze River. The equivalent spherical diameter of muscovite and biotite is calculated from their average thickness (~50 μm).

Yangtze sands have experienced complex multiple erosion, transport and deposition processes that may have led to a reduction in size of the older grains.

We suggest that the muscovite and biotite grain size - age trend is controlled by sediment multiple recycling. This multiple recycling interpretation is also supported by detrital zircon data. The Yangtze detrital zircon U–Pb ages (n = 993) record age populations of 2000–2600 Ma, 1600–2000 Ma, 600–000 Ma, 160–250 Ma and 0–60 Ma (Fig. 4e) (He et al., 2014; Yang et al., 2012). However, detrital biotite (n = 470) and muscovite (n = 687) grains from the Yangtze River only record age populations of 600–1000 Ma, 160–250 Ma and 0–60 Ma and lack older populations (2000–2500 Ma and 1600–2000 Ma). The absence of two older age components probably results from micas' lower closure temperature [Bt: 300–350 °C and Ms.: 350–425 °C (Harrison et al., 2009; McDougall and Harrison, 1999)] and lower resistance to physical and chemical weathering. The weathering has either completely destroyed the grain or reduced the grains size down to < 100 μm, which are not selected for age analyses in this study. Moreover, the age peaks of 600–1000 Ma and 160–250 Ma recorded by detrital biotites are lower (in relative probability and number) than corresponding peaks of muscovites (Fig. 4a and c), indicating the relatively lower physical and chemical durability, as also suggested by theoretical and empirical estimates (Kowalewski and Rimstidt, 2003) and slightly lower closure temperature.

5.2. Other factors

Other than multiple recycling, other possible factors that may explain the mica size - age relationship include (1) derivation from a particular type of rock and (2) numbers of analyses.

In principal, the observed trend can also be explained if the sources are composed of rocks with fine-grained older and large-grained younger micas. The Yangtze River basin comprises different rocks, ranging from Archean metamorphic rocks, Paleozoic carbonate, Mesozoic-Cenozoic igneous and siliciclastic rocks to Quaternary sediments (Yang et al., 2009). Most of these diverse rocks can provide muscovite and biotite grains to the Yangtze River system. Because of high erosion rate caused by active tectonism and heavy summer monsoon rains in the upper Yangtze (Hoang et al., 2010; Chappell et al., 2006), micas in the Yangtze River are mostly sourced from upstream

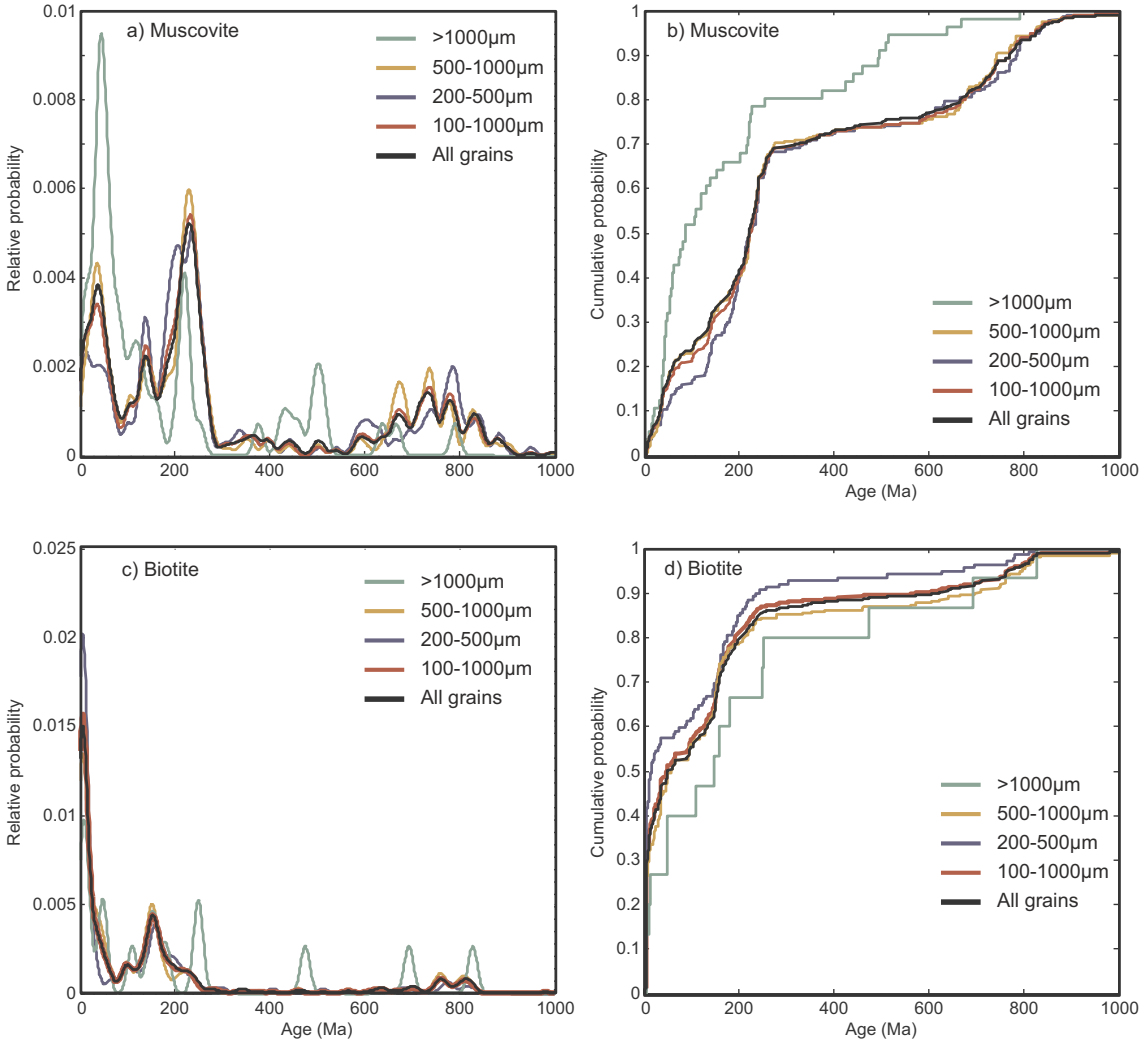

Fig. 5. Kernel density estimate (a and c) and cumulative probability plots of muscovite (a and b) and biotite (c and d) age distributions of the Yangtze data for different grain size windows. These plots show that the age distribution of a size window of 100–1000 μm is most representative for the entire data set.

areas (Hoang et al., 2010; Sun et al., 2016), which is composed of diverse rocks, including Mesoproterozoic metamorphic rocks, Mesozoic granites, Permian Emeishan basalts, Triassic flysch deposits and Mesozoic sandstones (He et al., 2013b). Such complex lithology distribution is inconsistent with the requirements of this interpretation (fine-grained older and large-grained younger rocks).

One might argue that the trend presented by detrital micas is caused by incomplete sampling of the population with ages of 500–1000 Ma (Ms: 130 of 686 and Bt: 52 of 470) to characterize grain size information. The number (130 and 52 analyses per sample) of analyses for the age range of 500–1000 Ma ensures a 95% certainty that no fraction > 4.6% and 9.7% was missed from the underlying detrital grain size population (Vermeesch, 2004). Therefore, our 130 muscovite and 52 biotite analyses in age range of 500–1000 Ma are sufficient to characterize the dominant grain size population. We therefore suggest that the relationship between detrital mica age and grain size is also unlikely to be caused by our finite number of analysis.

5.3. Evidence from other datasets

The grain size - age distribution relationship shown by our own Yangtze data can be confirmed by a reanalysis of mica ages derived from other major rivers. We compiled detrital mica $^{40}Ar/^{39}Ar$ data from current river sands of the Red River, Brahmaputra River, Quaternary glacial-diamict and glacial-marine detritus around the east Antarctic, and Cretaceous sandstones from Scotian basin, Canada (Fig. 6). ^{39}Ar signal size of each mica grain is a function of both neutron flux, K concentration and grain size. Although the K content of dated muscovite and biotite grains is not published in these studies, the significant variation in major element of muscovite and biotite is mainly controlled by the Tschermark substitution $(Mg,Fe)Si \rightleftharpoons Al_2$ (Miyashiro and Shido, 1985), Which is not related to K. The changes in K content of muscovite biotite is relatively narrow. Moreover, we have proved in Fig. 3a that the effect of K composition has a limited impact on ^{39}Ar variations.

Published data are obtained in different laboratories using different mass spectrometers. Because the sensitivity of these mass spectrometers is generally unknown/not published, it is not possible to convert the ^{39}Ar values of detrital mica grains from those studies into a uniform unit such as mole. We therefore used ^{39}Ar units as originally published (either fA, mV, or mol), but normalized for published J-values. However, this does not impede us from studying the grain size - age relationship. Samples from the Brahmaputra River (muscovite) show a boomerang-shape relationship between ^{39}Ar (grain size) and age (Fig. 6a), with older ages characterized by small sizes. Other detrital data (Red River, the Scotian basin and Antarctic) show similar ^{39}Ar (grain size) and age trend (Fig. 6b - d) to our Yangtze results (Fig. 4). We suggest the consistent detrital mica size – age relationship results from multi-recycling and associated weathering.

5.4. Implications

This study suggests that mica weathering and multiple recycles would result in a significant reduction of grain size for relatively older grains, highlighting the potential bias of grain size on detrital age component analyses. This is confirmed by variable mica age distributions for different grain-size classes, especially for grains > 1000 μm (Fig. 5). Therefore, selecting mica grain size of a suitable window for age analyses is crucial for reducing the bias on sampling of age populations.

In addition, micas display remarkable variation in grain size caused by hydraulic sorting (Garzanti et al., 2009) and/or different geodynamic settings in its source area (Resentini et al., 2013). Micas are deposit slower than similar size denser minerals due to their flat shape (Komar et al., 1984). Micas thus yield a wider grain size range in river sediment when compared with denser mineral like zircon (Garzanti et al., 2008, 2009). Potential bias caused by changes in geodynamic settings could be reduced by determination of the most appropriate size window for maximizing the identification of all age population in detrital micas in different geodynamic settings. The excel spreadsheet: MinSORTING devised to calculate the size-frequency distribution of any detrital component in sediment can be used for this purpose (Resentini et al., 2013). How to eliminate or minimize the hydrodynamic sorting effect on sediment provenance study using detrital minerals is still a matter of controversy. One widely used method is to narrow the size fraction for age analyses instead of the bulk sample (Morton et al., 2009; Weltje, 2004). However, Lawrence et al. (2011) and Garzanti et al. (2009) suggested that the "narrow-window" strategy cannot reflect the entire age information of all detrital zircon, and recommended to analyze a broader size range of grains ("wide-windows strategy"). It is probably more appropriate to combine the two different approaches by mixing detritus from different hydrodynamic sub-environments in the field and analyzing a broader size range in the lab (Garzanti et al., 2009) as we have done in this study.

Our results provide empirical insights into the size window for detrital mica age analyses. Due to great sensitivity improvement for $^{40}Ar/^{39}Ar$ dating equipment (e.g. Argus VI and Helix multi-collector mass spectrometer), the minimum grain size of mica for provenance study can reach 100 μm, even for ages < 10 Ma (Gemignani et al., 2019). Based on age distribution analyses for different grain size range (Fig. 5), mica age distributions of 100–1000 μm is the most similar to all dated grains. Other grain size windows like 200–500 μm, recommend by previous studies (Carrapa et al., 2004; Hodges et al., 2005), cover major populations, but underestimate relatively older ages (Fig. 5). We therefore suggest that it is better to cover 100–1000 μm detrital mica for provenance study.

6. Conclusions

In this study, we compile new and previously ^{39}Ar data and ages of detrital mica grains from the Yangtze River to characterize the effect of weathering and multiple recycles on age population analyses. We tested the suitability of ^{39}Ar beam intensity as a proxy for mica grain sizes. Our data show a trend that relatively older micas are generally smaller, and larger micas are younger. Such a finding is confirmed by a reanalysis of detrital mica data from the Asia (Red and Brahmaputra rivers), Scotian Basin (Canada) and Antarctic. This trend is likely a result of sediment multiple recycling, leading to more size reduction for older grains that have experienced more episodes of recycles than younger ones. Such a size bias on mica age population calls for an evaluation of a suitable size window that can yield representative detrital ages for the entire sample. Comparison of age distributions for various grain size windows (100–1000, 200–500, 500–1000 and > 1000 μm) shows that the 100–1000 μm micas cover all age components of all dated grains (100–2000 μm). We therefore suggest the 100–1000 μm size window for future detrital mica age analyses. Future work might investigate $^{40}Ar/^{39}Ar$ age distributions on grains < 100 μm, although that might be compromised by possible recoil effects on such small grains.

Supplementary data to this article can be found online at https://doi.org/10.1016/j.chemgeo.2019.119359.

Declaration of competing interest

The authors declare that they have no known competing financial interests or personal relationships that could have appeared to influence the work reported in this paper.

Acknowledgements

This study is financially supported by the National Natural Science Foundation of China (41671011, 41672355, 41772211, 41801003 and U1701641), the Guangdong Province Introduced Innovative R&D Team

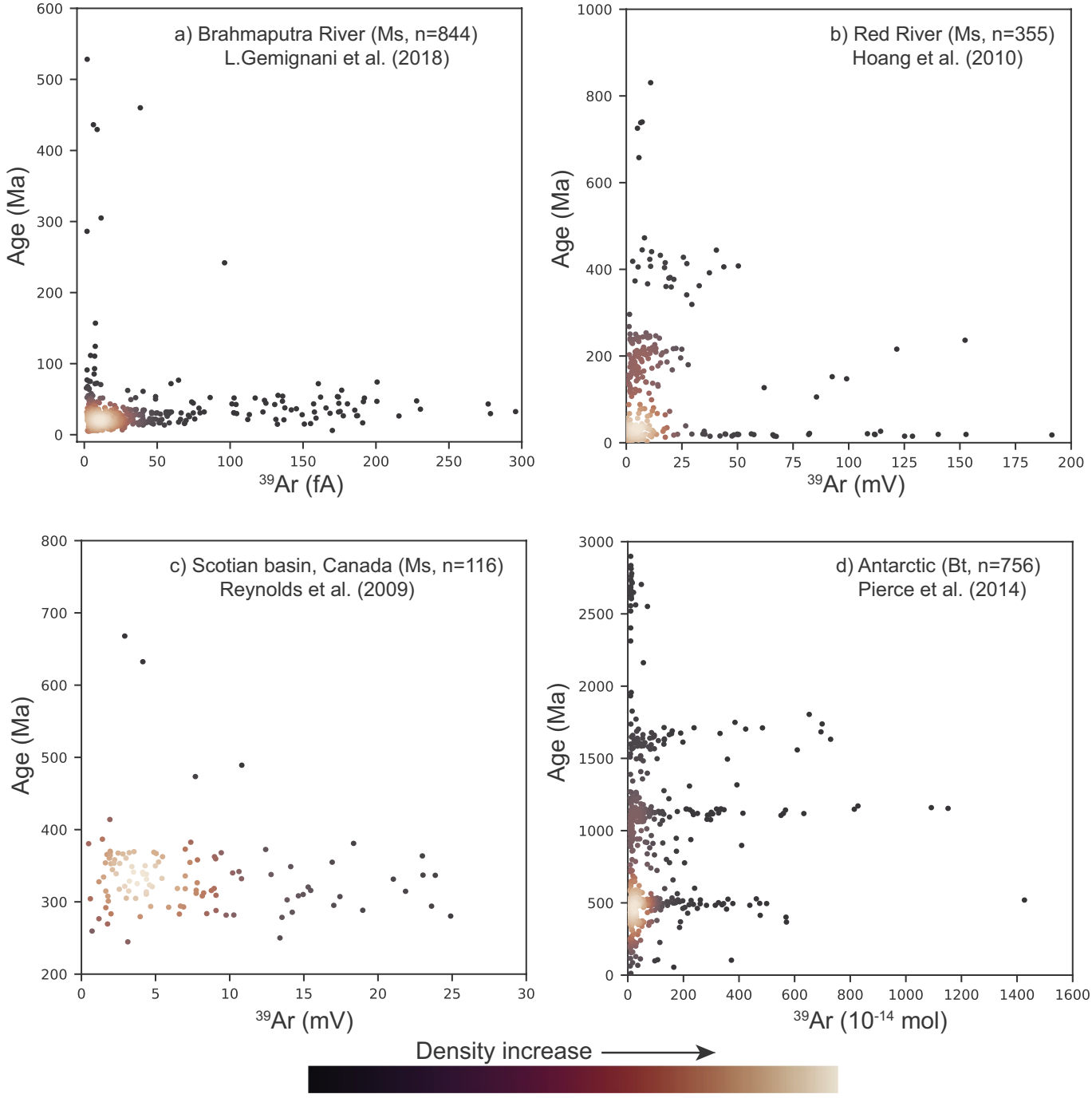

Fig. 6. Compiled detrital muscovite and biotite data from the Red and Brahmaputra rivers, Canada and Antarctic. The ^{39}Ar signal, with a unit as reported in original publications, is used as an index for grain size. Note, conversion of ^{39}Ar signals to our normalized ^{39}Ar signal in fA (and thus grainsize) is not possible due to lack of information on sensitivity in cited studies.

(2016ZT06N331) and the Fundamental Research Funds for the Central Universities (19lgjc03). This work was supported by the argon geochronology laboratory of the Vrije Universiteit Amsterdam. KK is supported by NWO-ALW grant 864.12.005. Roel van Elsas is acknowledged for his strategic help and support in the mineral separation laboratory at the Vrije Universiteit Amsterdam.

References

Alexandre, P., 2011. Comparison between grain size and multi-mineral ^{40}Ar/^{39}Ar thermochronology. Geochim. Cosmochim. Acta 75, 4260–4272.

Carrapa, B., Di Giulio, A., Wijbrans, J., 2004. The early stages of the Alpine collision: an image derived from the Upper Eocene–lower Oligocene record in the Alps–Apennines junction area. Sediment. Geol. 171, 181–203.

Chappell, J., Zheng, H.B., Fifield, K., 2006. Yangtse River sediments and erosion rates from source to sink traced with cosmogenic ^{10}Be: sediments from major rivers. Palaeogeogr. Palaeoclimatol. Palaeoecol. 241, 79–94.

Chetel, L.M., Simo, J.T., Singer, B.S., 2005. ^{40}Ar/^{39}Ar geochronology and provenance of detrital K-feldspars, Ordovician, Upper Mississippi Valley. Sediment. Geol. 182, 163–181.

China Geological Survey (CGS), 2004. Geological Map of China (1:2,500,000). China Geological Map Press, Beijing.

Clift, P.D., Carter, A., Campbell, I.H., Pringle, M.S., Van Lap, N., Allen, C.M., Hodges, K.V., Tan, M.T., 2006. Thermochronology of mineral grains in the Red and Mekong Rivers, Vietnam: provenance and exhumation implications for Southeast Asia. Geochem. Geophys. Geosyst. 7 (Q10005).

Dong, Y.P., Zhang, G.W., Neubauer, F., Liu, X.M., Genser, J., Hauzenberger, C., 2011.

Tectonic evolution of the Qinling orogen, China: review and synthesis. J. Asian Earth Sci. 41, 213–237.
Enkelmann, E., Ratschbacher, L., Jonckheere, R., Nestler, R., Fleischer, M., Gloaguen, R., Hacker, B.R., Zhang, Y.Q., Ma, Y.S., 2006. Cenozoic exhumation and deformation of northeastern Tibet and the Qinling: is Tibetan lower crustal flow diverging around the Sichuan Basin? Geol. Soc. Am. Bull. 118, 651–671.
Fan, D.D., Li, C.X., Kazumi, Y., Zhou, B.C., Li, B.H., Wang, Q., Yang, S.Y., Deng, B., Wu, G.X., 2005. Monazite age spectra in the Late Cenozoic strata of the Changjiang delta and its implication on the Changjiang run-through time. Sci. China. Ser. D Earth Sci. 48, 1718–1727.
Fuhrmann, U., Lippolt, H.J., Hess, J.C., 1987. Examination of some proposed K-Ar standards: $^{40}Ar/^{39}Ar$ analyses and conventional K-Ar data. Chemical Geology: Isotope Geoscience section 66, 41–51.
Garzanti, E., Andò, S., Vezzoli, G., 2008. Settling equivalence of detrital minerals and grain-size dependence of sediment composition. Earth Planet. Sci. Lett. 273, 138–151.
Garzanti, E., Andò, S., Vezzoli, G., 2009. Grain-size dependence of sediment composition and environmental bias in provenance studies. Earth Planet. Sci. Lett. 277, 422–432.
Gemignani, L., van der Beek, P., Braun, J., Najman, Y., Bernet, M., Garzanti, E., Wijbrans, J., 2018. Downstream evolution of the thermochronologic age signal in the Brahmaputra catchment (eastern Himalaya): implications for the detrital record of erosion. Earth Planet. Sci. Lett. 499, 48–61.
Gemignani, L., Kuiper, K.F., Wijbrans, J.R., Sun, X., Santato, A., 2019. Improving the precision of single grain mica $^{40}Ar/^{39}Ar$-dating on smaller and younger muscovite grains: application to provenance studies. Chem. Geol. 511, 100–111.
Gwiazda, R.H., Hemming, S.R., Broecker, W.S., Onsttot, T., Mueller, C., 1996. Evidence from $^{40}Ar/^{39}Ar$ ages for a Churchill Province source of ice-rafted amphiboles in Heinrich layer 2. J. Glaciol. 42, 440–446.
Haines, P.W., Turner, S.P., Kelley, S.P., Wartho, J.A., Sherlock, S.C., 2004. $^{40}Ar/^{39}Ar$ dating of detrital muscovite in provenance investigations: a case study from the Adelaide Rift complex, South Australia. Earth Planet. Sci. Lett. 227, 297–311.
Harrison, T.M., Célérier, J., Aikman, A.B., Hermann, J., Heizler, M.T., 2009. Diffusion of ^{40}Ar in muscovite. Geochim. Cosmochim. Acta 73, 1039–1051.
He, M.Y., Zheng, H.B., Clift, P.D., 2013a. Zircon U–Pb geochronology and Hf isotope data from the Yangtze River sands: implications for major magmatic events and crustal evolution in Central China. Chem. Geol. 360-361, 186–203.
He, M.Y., Zheng, H.B., Huang, X.T., Jia, J.T., Li, L., 2013b. Yangtze River sediments from source to sink traced with clay mineralogy. J. Asian Earth Sci. 69, 60–69.
He, M.Y., Zheng, H.B., Bookhagen, B., Clift, P.D., 2014. Controls on erosion intensity in the Yangtze River basin tracked by U-Pb detrital zircon dating. Earth Sci. Rev. 136, 121–140.
Hoang, L.v., Clift, P.D., Mark, D., Zheng, H.B., Mai Thanh, T., 2010. Ar-Ar muscovite dating as a constraint on sediment provenance and erosion processes in the Red and Yangtze River systems, SE Asia. Earth and Planetary Science Letters 295, 379–389.
Hodges, K.V., Ruhl, K.W., Wobus, C.W., Pringle, M.S., 2005. $^{40}Ar/^{39}Ar$ thermochronology of detrital minerals. In: Low-Temperature Thermochronology: Techniques, Interpretations, and Applications, pp. 239–257.
Jia, J.T., Zheng, H.B., Huang, X.T., Wu, F.Y., Yang, S.Y., Wang, K., He, M.Y., 2010. Detrital zircon U-Pb ages of Late Cenozoic sediments from the Yangtze delta: implication for the evolution of the Yangtze River. Chin. Sci. Bull. 55, 1520–1528.
Komar, P.D., Baba, J., Bingquan, C., 1984. Grain-size analyses of mica within sediments and the hydraulic equivalence of mica and quartz. J. Sediment. Res. 54, 1379–1391.
Kowalewski, Michał, Rimstidt, J. Donald, 2003. Average lifetime and age spectra of detrital grains: toward a unifying theory of sedimentary particles. The Journal of Geology 111, 427–439.
Kuiper, K., Deino, A., Hilgen, F., Krijgsman, W., Renne, P., Wijbrans, J., 2008. Synchronizing rock clocks of Earth history. Science 320, 500–504.
Lawrence, R.L., Cox, R., Mapes, R.W., Coleman, D.S., 2011. Hydrodynamic fractionation of zircon age populations. Geol. Soc. Am. Bull. 123, 295–305.
Malusà, M.G., Carter, A., Limoncelli, M., Villa, I.M., Garzanti, E., 2013. Bias in detrital zircon geochronology and thermochronometry. Chem. Geol. 359, 90–107.
Malusà, M.G., Resentini, A., Garzanti, E., 2016. Hydraulic sorting and mineral fertility bias in detrital geochronology. Gondwana Res. 31, 1–19.
Markley, M.J., Teyssier, C., Cosca, M., 2002. The relation between grain size and $^{40}Ar/^{39}Ar$ date for Alpine white mica from the Siviez-Mischabel Nappe, Switzerland. J. Struct. Geol. 24, 1937–1955.
McDougall, I., Harrison, T.M., 1999. Geochronology and Thermochronology by the $^{40}Ar/^{39}Ar$ Method. Oxford University Press on Demand.
Miyashiro, A., Shido, F., 1985. Tschermak substitution in low-and middle-grade pelitic schists. J. Petrol. 26, 449–487.
Morton, A., Hallsworth, C., Strogen, D., Whitham, A., Fanning, M., 2009. Evolution of provenance in the NE Atlantic rift: the Early–Middle Jurassic succession in the Heidrun Field, Halten Terrace, offshore Mid-Norway. Mar. Pet. Geol. 26, 1100–1117.
Parrish, R.R., 1990. U–Pb dating of monazite and its application to geological problems. Can. J. Earth Sci. 27, 1431–1450.
Pierce, E., Hemming, S., Williams, T., van de Flierdt, T., Thomson, S., Reiners, P.W., Gehrels, G.E., Brachfeld, S., Goldstein, S., 2014. A comparison of detrital U – Pb zircon, $^{40}Ar/^{39}Ar$ hornblende, $^{40}Ar/^{39}Ar$ biotite ages in marine sediments off East Antarctica: Implications for the geology of subglacial terrains and provenance studies. Earth Sci. Rev. 138, 156–178.
Reid, A.J., Wilson, C.J.L., Phillips, D., Liu, S., 2005. Mesozoic cooling across the Yidun Arc, central-eastern Tibetan Plateau: a reconnaissance $^{40}Ar/^{39}Ar$ study. Tectonophysics 398, 45–66.
Resentini, A., Malusà, M.G., Garzanti, E., 2013. MinSORTING: an Excel® worksheet for modelling mineral grain-size distribution in sediments, with application to detrital geochronology and provenance studies. Comput. Geosci. 59, 90–97.
Reynolds, P.H., Pe-Piper, G., Piper, D.J., Grist, A., 2009. Single-grain detrital-muscovite ages from Lower Cretaceous sandstones, Scotian basin, and their implications for provenance. Bull. Can. Petrol. Geol. 57, 63–80.
Roger, F., Jolivet, M., Malavieille, J., 2010. The tectonic evolution of the Songpan-Garzê (North Tibet) and adjacent areas from Proterozoic to present: a synthesis. J. Asian Earth Sci. 39, 254–269.
Shao, L., Li, C.A., Yuan, S.Y., Kang, C.G., Wang, J.T., Li, T., 2012. Neodymium isotopic variations of the late Cenozoic sediments in the Jianghan Basin: Implications for sediment source and evolution of the Yangtze River. J. Asian Earth Sci. 45, 57–64.
Shu, L.S., Faure, M., Yu, J.H., Jahn, B.M., 2011. Geochronological and geochemical features of the Cathaysia block (South China): new evidence for the Neoproterozoic breakup of Rodinia. Precambrian Res. 187, 263–276.
Sircombe, K.N., Bleeker, W., Stern, R.A., 2001. Detrital zircon geochronology and grain-size analysis of a ~2800 Ma Mesoarchean proto-cratonic cover succession, Slave Province, Canada. Earth Planet. Sci. Lett. 189, 207–220.
Stuart, F.M., Bluck, B.J., Pringle, M.S., 2001. Detrital muscovite $^{40}Ar/^{39}Ar$ ages from Carboniferous sandstones of the British Isles: provenance and implications for the uplift history of orogenic belts. Tectonics 20, 255–267.
Sun, X.L., Li, C.A., Kuiper, K.F., Zhang, Z.J., Gao, J.H., Wijbrans, J.R., 2016. Human impact on erosion patterns and sediment transport in the Yangtze River. Glob. Planet. Chang. 143, 88–99.
Sun, X.L., Li, C.A., Kuiper, K.F., Wang, J.T., Tian, Y.T., Vermeesch, P., Zhang, Z.J., Zhao, J.X., Wijbrans, J.R., 2018. Geochronology of detrital muscovite and zircon constrains the sediment provenance changes in the Yangtze River during the late Cenozoic. Basin Res. 30, 636–649.
Uddin, A., Hames, W.E., Zahid, K.M., 2010. Laser $^{40}Ar/^{39}Ar$ age constraints on Miocene sequences from the Bengal basin: implications for middle Miocene denudation of the eastern Himalayas. Journal of Geophysical Research-Solid Earth 115. https://doi.org/10.1029/2009JB006401.
Újvári, G., Klötzli, U., Kiraly, F., Ntaflos, T., 2013. Towards identifying the origin of metamorphic components in Austrian loess: insights from detrital rutile chemistry, thermometry and U–Pb geochronology. Quat. Sci. Rev. 75, 132–142.
Uunk, B., Brouwer, F., ter Voorde, M., Wijbrans, J., 2018. Understanding phengite argon closure using single grain fusion age distributions in the Cycladic Blueschist Unit on Syros, Greece. Earth Planet. Sci. Lett. 484, 192–203.
Vermeesch, P., 2004. How many grains are needed for a provenance study? Earth Planet. Sci. Lett. 224, 441–451.
Vezzoli, G., Garzanti, E., Limonta, M., Andò, S., Yang, S.Y., 2016. Erosion patterns in the Changjiang (Yangtze River) catchment revealed by bulk-sample versus single-mineral provenance budgets. Geomorphology 261, 177–192.
Wang, J.T., Li, C.A., Yang, Y., Shao, L., 2010. Detrital zircon geochronology and provenance of core sediments in Zhoulao Town, Jianghan Plain, China. J. Earth Sci. 21, 257–271.
Weislogel, A.L., Graham, S.A., Chang, E.Z., Wooden, J.L., Gehrels, G.E., Yang, H.S., 2006. Detrital zircon provenance of the Late Triassic Songpan-Ganzi complex: sedimentary record of collision of the North and South China blocks. Geology 34, 97–100.
Weislogel, A.L., Graham, S.A., Chang, E.Z., Wooden, J.L., Gehrels, G.E., 2010. Detrital zircon provenance from three turbidite depocenters of the Middle-Upper Triassic Songpan-Ganzi complex, central China: record of collisional tectonics, erosional exhumation, and sediment production. Geol. Soc. Am. Bull. 122, 2041–2062.
Weltje, G.J., 2004. A quantitative approach to capturing the compositional variability of modern sands. Sediment. Geol. 171, 59–77.
Wijbrans, J.R., Pringle, M.S., Koppers, A.A.P., Scheveers, R., 1995. Argon geochronology of small samples using the Vulkaan argon laser probe. R. Neth. Acad. Sci. 98, 185–218.
Wu, W.H., Xu, S.J., Yang, J.D., Yin, H.W., Tao, X.C., 2009. Sr fluxes and isotopic compositions in the headwaters of the Yangtze River, Tongtian River and Jinsha River originating from the Qinghai–Tibet Plateau. Chem. Geol. 260, 63–72.
Xu, Z.Q., Hou, L.W., Wang, Z.X., Fu, X.F., Huang, M.H., 1992. Orogenic Processes of the Songpan-Garze Orogenic Belt of China. Geol. Publ. House, Beijing, pp. 1–235.
Yan, Z.K., Tian, Y.T., Li, R., Vermeesch, P., Sun, X.L., Li, Y., Rittner, M., Carter, A., Shao, C.J., Huang, H., Ji, X.T., 2019. Late Triassic tectonic inversion in the upper Yangtze Block: insights from detrital zircon U–Pb geochronology from South-Western Sichuan Basin. Basin Res. 31, 92–113.
Yang, S.Y., Wang, Z.B., Guo, Y., Li, C.X., Cai, J.G., 2009. Heavy mineral compositions of the Changjiang (Yangtze River) sediments and their provenance-tracing implication. J. Asian Earth Sci. 35, 56–65.
Yang, S.Y., Zhang, F., Wang, Z.B., 2012. Grain size distribution and age population of detrital zircons from the Changjiang (Yangtze) river system, China. Chem. Geol. 296–297, 26–38.
Zhang, Z.J., Tyrrell, S., Li, C.A., Daly, J.S., Sun, X.L., Blowick, A., Lin, X., 2016. Provenance of detrital K-feldspar in Jianghan Basin sheds new light on the Pliocene – Pleistocene evolution of the Yangtze River. Geol. Soc. Am. Bull. 128 (9–10), 1339–1351.